JNeurosci
THE JOURNAL OF NEUROSCIENCE

Research Articles: Neurobiology of Disease

Continuous Monitoring of Tau-Induced Neurotoxicity in Patient-Derived iPSC-Neurons

https://doi.org/10.1523/JNEUROSCI.2590-20.2021

Cite as: J. Neurosci 2021; 10.1523/JNEUROSCI.2590-20.2021

Received: 6 October 2020
Revised: 12 February 2021
Accepted: 19 February 2021

Title: Continuous monitoring of tau-induced neurotoxicity in patient-derived iPSC-neurons

Abbreviated Title: Tau-induced neurotoxicity in human iPSC-neurons

Derek H. Oakley M.D., Ph.D.[1,3,4,5], Naomi Klickstein B.S. [1,2], Caitlin Commins B.S. [1,2], Mirra Chung[1,2]M.S., Simon Dujardin Ph.D. [1,2], Rachel E. Bennett Ph.D. [1,2], Bradley T. Hyman M.D., Ph.D. [1,2,5] & Matthew P. Frosch M.D., Ph.D. [1,3,4,5]

[1]Harvard Medical School
[2]Massachusetts General Hospital Department of Neurology
[3]Massachusetts General Hospital Department of Pathology
[4]C.S. Kubik Laboratory for Neuropathology
[5]Massachusetts Alzheimer's Disease Research Center

* Derek H. Oakley M.D., Ph.D.
Email: doakley@partners.org

This PDF file includes 42 total pages:

Main Text.
Figures 1 to 6.
Table 1.
Extended Data Figures: 1-1, 1-2, 2-1, 3-1, 3-2, 4-1, 5-1, 5-2, & 5-3.
Legends for Movies 1, 2, 3.

Word counts:

Abstract: 217
Introduction: 750
Discussion: 1709 (1362 prior to revision)

Conflicts of Interest: The authors declare no competing financial interests.

Acknowledgements: We would like to acknowledge Marc Diamond (University of Texas Southwestern) for the gift of TauRD reporter plasmids and Nicole Deglon (CHUV Lausanne) for the gift of lentiviral packaging plasmids. iPSC lines were provided by the Massachusetts Alzheimer's Disease Research Center (1P30AG062421-01) and were initially generated from patient samples in collaboration with Ricardo Dolmesch at the Novartis Institutes for BioMedical Research, Boston, MA.

Abstract: Tau aggregation within neurons is a critical feature of Alzheimer disease (AD) and related tauopathies. It is believed that soluble pathologic tau species seed the formation of tau aggregates in a prion-like manner and propagate through connected neurons during the progression of disease. Both soluble and aggregated forms of tau are thought to have neurotoxic properties. In addition, different strains of misfolded tau may cause differential neurotoxicity. In this work, we present an accelerated human neuronal model of tau-induced neurotoxicity that incorporates both soluble tau species and tau aggregation. Utilizing patient-derived induced pluripotent stem cell (iPSC) neurons expressing a tau aggregation biosensor, we develop a cell culture system that allows continuous assessment of both induced tau aggregation and neuronal viability at single-cell resolution for periods of over one week. We show that exogenous tau "seed" uptake, as measured by tau repeat domain (TauRD) reporter aggregation, increases the risk for subsequent neuronal death *in vitro*. These results are the first to directly visualize neuronal TauRD aggregation and subsequent cell death in single human iPSC-neurons. Specific morphologic strains or patterns of TauRD aggregation are then identified and associated with differing neurotoxicity. Furthermore, we demonstrate that familial AD iPSC-neurons expressing the PSEN1 L435F mutation exhibit accelerated TauRD aggregation kinetics and a tau strain propagation bias when compared to control iPSC-neurons.

Significance Statement: Neuronal intracellular aggregation of the microtubule binding protein tau occurs in Alzheimer disease and related neurodegenerative tauopathies. Tau aggregates are believed to spread from neuron-to-neuron via prion-like misfolded tau seeds. Our work develops a human neuronal live-imaging system to visualize seeded tau aggregation and tau-induced neurotoxicity within single neurons. Using an aggregation-sensing tau reporter, we find that neuronal uptake and propagation of tau seeds reduces subsequent survival. In addition, human iPSC-neurons carrying an Alzheimer's disease-causing mutation in presenilin-1 undergo tau seeding more rapidly than control iPSC-neurons. However, they do not show subsequent differences in neuronal survival. Finally, specific morphologies of tau aggregates are associated with increased neurotoxicity.

Main Text:

Introduction:

Pathologic phosphorylation and subsequent aggregation of the microtubule binding protein tau (MAPT) is believed to play a central role in driving cognitive decline in Alzheimer disease (AD) and related tauopathies. In these diseases, hyperphosphorylated tau species are thought to adopt a corrupted, aggregate-prone conformation that seeds misfolding of native tau, leading to prion-like spread of tau aggregates throughout the brain(Holmes et al., 2014; Kaufman et al., 2016; Furman et al., 2017; DeVos et al., 2018). In addition, these tau "seeds" can propagate as distinct strains of misfolded protein, both within single patients and across different tauopathies(Mudher et al., 2017). In AD, Amyloid-β (Aβ) species promote tau hyperphosphorylation and may also aid in spreading tau pathology by other mechanisms(Choi et al., 2014; Bennett et al., 2017; He et al., 2018).

There is strong clinicopathologic evidence that tau aggregation correlates with neuronal loss and cognitive decline both in AD(Arriagada et al., 1992; Nelson et al., 2012; Brier et al., 2016) and in tau transgenic animals(Santacruz et al., 2005; Wirths and Bayer, 2010; DeVos et al., 2017). However, whether tau aggregation is itself toxic or simply an epiphenomenon associated with toxic soluble tau species remains a matter of debate.

In order to visualize and measure proteopathic tau "seeds", several different tau aggregation biosensor molecules have been developed. These reporters are composed of fluorescent molecules or other protein epitopes fused to the repeat domain of tau (TauRD) which has been altered to carry at least one pro-aggregation mutation such as MAPT P301L. Importantly, tau aggregation biosensors are designed to aggregate only in the presence of tau seeds, not spontaneously. The most established such model, composed of HEK cells expressing a TauRD biosensor, has been used to demonstrate the presence of tau seeds within donated human AD brain tissues as well as animal models of tauopathy (Holmes et al., 2014; Dujardin et al., 2020). Work with TauRD biosensors shows that seed-competent misfolded

tau consists of high molecular weight phosphorylated oligomers and precedes neurofibrillary tangles in AD patient brain tissues (Holmes et al., 2014; Takeda et al., 2015; Takeda et al., 2016; Kaufman et al., 2017; Nobuhara et al., 2017; DeVos et al., 2018; Dujardin et al., 2020).

The HEK TauRD reporter model has also been used to identify and propagate distinct morphologic strains of tau seeds from patients with AD and other tauopathies(Sanders et al., 2014; Kaufman et al., 2016; Kaufman et al., 2017). These strain morphologies have been described in HEK cells, but have not been observed in human neuronal cultures (Sanders et al., 2014). Interestingly, some morphologic strains of TauRD aggregates cannot be propagated in HEK cells due to apparent strain-specific cytotoxicity (Sanders et al., 2014).

In this study, we sought to create an accelerated human neuronal model of tau-induced neurotoxicity that incorporates both soluble tau species and seeded TauRD aggregation. We developed a model based on patient-derived iPSC-neurons that shows clear tau aggregate seeding and tau-induced toxicity after misfolded tau is taken up from the media. To accomplish this, we stably expressed a non-spontaneously-aggregating TauRD biosensor in iPSC-neurons and then seeded TauRD aggregation using tau seeds derived from mice carrying the MAPT P301L mutation (rTg4510) (Ramsden et al., 2005; Santacruz et al., 2005). Utilizing longitudinal *in-vitro* live-imaging and a custom single cell tracking workflow, we were then able to compare neuronal survival between iPSC-neurons that aggregated the TauRD construct and adjacent non-aggregating cells in the same well. This approach allows us to assess toxicity downstream of tau uptake and aggregation, controlling both for expression of the TauRD construct and overall exposure to seed-competent tau.

The model also permits exploration of patient- and strain-specific neuronal responses to toxic tau species. Our recent studies have demonstrated that iPSC-neurons carrying the familial AD-causing PSEN1 L435F mutation show increased Aβ43, Aβ43/40 and Aβ42/40 ratios as well as increased phosphorylated tau compared to control iPSC-neurons (Oakley et al., 2020). Based on prior reports showing that longer-length Aβ species promote TauRD seeding (Bennett et al., 2017), we hypothesized

that that familial AD-iPSCs would demonstrate accelerated seeding after addition of exogenous tau species. Our observations support this notion. Following TauRD aggregation, there is equivalent rate of subacute neuronal toxicity observed in both the PSEN1 mutant and control lines, suggesting that any effect of elevated Aβ43 in this model is on tau aggregation, rather than a direct effect on toxicity. Finally, we identify specific morphologic strains or patterns of TauRD reporter aggregates that appear to occur at different rates in the two cell lines and, interestingly, correlate with neuronal survival.

Materials & Methods:

Plasmids and lentiviral production: pLVX-TetOne-Puro-hNGN2 (Clontek) lentiviral plasmid for constitutive expression of puromycin resistance and doxycycline-inducible expression of human NGN2 was a gift from K.A. Worringer (Novartis Institutes for BioMedical Research). Plenti-UBC-TauRD(P301L)-CFP-2A-TauRD(P301L)-YFP lentiviral plasmid was generated from pLenti-UBC (Invitrogen) using pcDNA3.1-TauRD(P301L)-CFP-2A-TauRD(P301L)-YFP (TauFRET2)(Nicholls et al., 2017) . VSVG-pseudotyped lentivirus was prepared and concentrated via ultracentrifugation as previously described (Dujardin et al., 2014).

Mouse brain lysate preparation: Mouse brain lysates were prepared as previously described (Bennett et al., 2017). Whole brains from 12-month-old rTg4510 and control littermate mice (Jackson Laboratories) were homogenized by dounce-homogenization in 5x weight by volume ice-cold PBS-/- (Gibco) with protease inhibitor (Cell signaling #5871S) followed by centrifugation at 3k x g for 10min. The resulting pellets were resuspended in 500 µL PBS-/- with protease inhibitor and sonicated on ice, then re-centrifuged at 3k x g. The resulting supernatant was used as seed material.

iPSC lentiviral transduction neuronal differentiation: Lentiviral transduction was performed as previously reported with minor modifications (Oakley et al., 2020). To generate iPSCs expressing the TauRD reporter along with inducible NGN2 lentivirus, 300K iPSCs were plated on one well of 6-well plate in the presence of thiazovivin and co-infected with pLVX-TetOne-Puro-hNGN2 and Plenti-UBC-

TauRD(P301L)-CFP-2A-TauRD(P301L)-YFP lentivirus O/N at 24 hours after plating. Following initial lentiviral transduction, cells were passaged with Accutase treatment into a 10 cm plate and selected with 5 µg/mL puromycin after 24 hours (Gibco A11138-03). Puromycin-resistant iPSCs were then expanded and kept under 5 µg/mL puromycin selection to limit lentiviral silencing.

Our initial approach to lentiviral infection was to use a TauRD-CFP_2A_TauRD-YFP split construct commonly employed to produce a CFP-to-YFP FRET signal upon tauRD aggregation (Holmes et al., 2014; Nicholls et al., 2017). However, after infecting iPSCs with lentivirus encoding ubiquitously expressed TauRD-CFP_2A_TauRD-YFP, we observed YFP expression only and a complete lack of CFP on flow cytometry (see Extended Data Figure 1-1C). Given the high level of sequence homology between the TauRD-CFP and TauRD-YFP halves of the construct, this result is most likely due to recombination during reverse transcription and has been observed in prior studies (Komatsubara et al., 2015). Furthermore, this was not the case in HEK293 cells infected with similar constructs, which showed both YFP-only, and CFP/YFP double-positive cells (data not shown). Ultimately, our approach resulted in iPSCs expressing only the TauRD-YFP half of the construct, precluding the use of FRET to measure TauRD aggregation. Fortunately, the TauRD-YFP signal alone can be used to monitor TauRD aggregation via standard epifluorescent or confocal microscopy.

iPS-neurons were subsequently differentiated using doxycycline-driven expression of hNGN2 combined with SMAD and WNT inhibition as previously described, with the continued use of antimitotic for the duration of experiments to reduce dividing non-neuronal cells during live-imaging (Nehme et al., 2018; Oakley et al., 2020). At Day 0 (D0), NGN2 inducible iPSCs were passaged as single cells with Accutase and plated at 400kcells per well on Matrigel coated 6-well plates in mTeSR medium with rock inhibitor (thiazovivin, 1µM, EMD millipore). Doxycycline (2ug/mL, Sigma) was added on plating at D0 to induce NGN2 expression and maintained in culture medium thereafter. On D1, medium was switched to N2 media (DMEM:F12 (Gibco), Glutamax (1%, Gibco), Dextrose (0.3%, EM science), N2 (1%, Gibco)) supplemented with SB431542 (10 uM, Tocris), LDN-193189 (100 nM, Stemgent), XAV939 (2

μM, Stemgent), and doxycycline. On D2, cells were fed with N2 medium with SB/XAV/LDN at one half the concentration of D1 and doxycycline at full concentration. On D3, cells were fed with N2 medium supplemented with NT3 (10 ng/mL, PreproTech), BDNF (10 ng/mL R&D), GDNF (10 ng/mL, R&D), and doxycycline. On D4, cells were switched to NBM media (Neurobasal Medium, minus phenol red (Gibco), Glutamax (1%), Dextrose (0.3%), NEAA (0.5%, Gibco), and B27 (2%, Gibco)) supplemented with NT3, BDNF, GDNF, doxycycline, and the antimitotic FUDR (10μM, Sigma). Cells were fed with D4 media every 2-3 days until day 14, and cells were fed weekly thereafter. Beginning at D8, 2% horse serum (Gibco 26-050-088) was added to media to improve neuronal survival. For live-imaging and immunohistochemistry, differentiating neurons were passaged at D7 using accutase treatment and plated onto 96-well plates (20k cells/well) with 2% horse serum added at this time to improve survival. 96-well plates were pre-coated with Poly-D-Lysine (Corning 356640) and further coated with Laminin (10 μg/mL, Sigma), fibronectin (2 μg/mL, Sigma), and Matrigel (2.5x, Corning) in DMEM:F12 for 3hr at RT.

Species and sex studied: The human iPSC lines used in these studies are all female (See Table 1).

Live imaging experiments: iPS-neurons expressing TauRD-YFP reporter were cultured as described above and plated at day 7 of differentiation onto 96-well plates, where they were allowed to mature until day 14 to 17 of differentiation prior to live-imaging experiments. 4 hours prior to imaging, a far-red nuclear dye (NucSpot 650, Biotium 40082) was added to the media to allow time-lapse visualization of nuclear morphology and nuclear fragmentation associated with cell death (1/1000 in DMSO). At this time, DNAse1 (Worthington LK003170) was also added at a final concentration of 0.148 units/μL to pre-digest dead cell nuclei, which can otherwise obscure the signal from live nuclei. Within one imaging interval prior to the start of imaging (2 hours), tau seed-containing and control brain lysates were added to the culture media at 1-10 μg of total protein into 150μL media/well. Epifluorescent live-imaging was then begun using a temperature and CO_2 controlled microscope (Cytation5, Biotek) with images taken every 2 hours for 7 days. For each well imaged, a 4x4 or 5x5 grid of 10x images was acquired.

Following live-imaging experiments, media was harvested, and cells were fixed for immunohistochemistry.

Flow cytometry: Flow cytometry to measure expression of TauRD reporter was performed using a MACSQuant VYB Flow Cytometer (Miltenyi Biotec, Bergisch Gladbach, Germany) equipped with VivoBlue (CFP) and FITC (YFP) imaging channels.

iPSC/iPSC-neuron immunocytochemistry and microscopy: Immunocytochemistry was performed as previously described (Oakley et al., 2020). Stained cells were imaged on a Biotek Cytation 5 or ImageXpress Micro Confocal microscope. YFP staining was performed using a cross-reacting chicken anti-GFP antibody (Abcam ab13970, 1:500), PHF1 anti-phospho-tau antibody (1:200) was a gift from the Davies Lab. Immunocytochemistry for Tuj1 and cortical layer markers was performed using antibodies against Tuj1 (Aves TUJ, 1:500), CUX1/CUTL1 (Abcam ab54583, 1:300), Brn2 (Abcam ab1377469, 1:300), Ctip2 (Abcam ab18465, 1:100), and Tbr1 (Abcam ab31940, 1:1000).

Image analysis and neuronal survival: Following live-imaging experiments, resulting images were processed, and neuronal survival scored using a toolset of custom NIH ImageJ macros. The macro toolset facilitates image pre-processing (background subtraction, time-lapse image alignment, fluorescent channel overlay), manual cell scoring of morphologically identified neurons (frame-by-frame assignment of cell survival, cell position, and aggregate formation), censoring of cells that leave the field of view, and recording results. Measurement of TauRD reporter seed formation in neurites in Figure 3 was performed using Cytation Gen3 software to identify objects 0.1 to 4µm in size >10000 grey levels above local background. Larger bright areas were excluded from the analysis to avoid over-counting within clusters of cells (See Extended Data Figure 2-1)

Automated WEKA segmentation was used to measure neurite density of iPSC-neurons. Trainable WEKA segmentation (V23.2.32) with a fast random forest classifier was used to classify GFP images into 3 compartments: Cell Bodies, Neurites, and Background. Training features used were: Gaussian

blur, Hessian, membrane projections, Sobel filter, and Difference of Gaussians with settings membrane thickness=1, membrane patch size=19, and sigma 1-16. A probability map of the neurite compartment was thresholded using NIH ImageJ to produce object-level information for neurite area measurements.

Percent Tuj1 positivity following live-imaging experiments was determined using Gen5 software (Biotek) following immunohistochemistry as described above. Cortical layer marker expression in neurons was analyzed using custom NIH ImageJ macros. Neuronal nuclei were first identified and annotated based on Tuj1-positivity and DAPI staining in a manner analogous to neuronal identification in live imaging experiments. This was done to ensure similarity to the populations analyzed in neuronal seeding and survival assays. Subsequently, individual neuronal nuclei were segmented from images, DAPI stain was used to mask nuclear compartments, and underlying RFP and CY5 positivity was measured using thresholding and particle analysis in NIH ImageJ. Results were then processed and visualized using Excel and R Studio.

Strain morphologies in seeded iPSC neurons were identified in a blinded fashion using morphologic categories as described (Sanders et al., 2014). 70 x 70 pixel images of tracked neurons with aggregates (YFP-channel only) were extracted and displayed as animated Z-stacks, restricted to frames starting at the time of aggregate formation to either the end of the experiment or cell death, whichever occurred sooner. Images were chosen randomly from all tracked neurons in 4 biological replicates. Cell line or neuronal lifespan was not was not viewable at the time of scoring. Choices of strains were “Ordered”, “Disordered”, “Speckles”, “Toxic”, “Other”, or “Unclassifiable”. “Unclassifiable” cells were subsequently excluded from analysis. The “Speckles” category was interpreted to mean prominent nuclear speckles as opposed to diffuse cytoplasmic speckling, which fell into the category of “Disordered”. Subsequent data analysis was performed in R Studio.

Brain lysate labeling and uptake assay: rTg4510 lysate was labeled with Alexa 647-NHS (ThermoFisher A37573) for 1hr at RT, according to the manufacturer’s instructions. The resulting mixture was then dialyzed in PBS O/N at 4C using a 2KD cutoff membrane (ThermoFisher 66205) to

remove unbound label. Labeled lysate was added to iPSC-neurons at 10µg of total protein per well and subsequently let incubate for 5 days, prior to fixation with 4% paraformaldehyde. Fixed neurons were labeled with DAPI and imaged on an ImageXpress Micro Confocal microscope in DAPI, FITC (YFP), and CY5 (647) cannels at 20x with 20 z-planes. Resulting maximal intensity projection whole-well tiled images were then analyzed using custom ImageJ macros. Neurons were identified and outlined in the YFP channel and assigned to either aggregate-bearing or non-aggregate-bearing classes. The mean 647 intensity in the neuronal soma and DAPI-labeled nuclear compartment was subsequently measured manually for each neuron. Results were analyzed in R studio using the ggplot2 library.

ELISA: ELISA measurements of Aβ species were run according to the manufacturer's instructions as previously described (Oakley et al., 2020). Human Aβ 1-40 (WAKO 298-64601), human Aβ 1-42 (WAKO 296-64401) and Human Aβ 1-43 (IBL 27710) were measured separately in centrifuged cell supernatant. Assay plates were analyzed using a Perkin Elmer Wallac Victor2 at 450nM.

Western Blot: Cells were harvested at D28 on ice into ice-cold RIPA buffer with protease inhibitor (Cell signaling #5871S) using a cell scraper. Subsequently, cells were lysed with 10 passes using insulin syringes and pelleted for 10min x 10kg at 4C. Western blots were performed on 10ug samples of soluble supernatants using the Invitrogen NuPage Novex Gel System according to the manufacturer's instructions. Fluorescent secondary antibodies were used at a concentration of 1:5000. Blots were imaged on a LI-COR Odyssey system and analyzed using LI-COR Image Studio.

Statistical Methods: Calculation of standard deviation, standard error, and two-tailed Student's and Welch two sample T-tests, were performed using Microsoft Excel Analysis ToolPak and R. Kaplan-Meier survival curves, log-rank tests, and Cox-proportional hazards were calculated using the R survminer package. Two-way ANOVA and R^2 values were calculated using the R rstatix package.

Results:

TauRD reporter expression in Control and fAD human iPSC-derived neurons.

Two iPSC lines derived from brain donors at the time of autopsy were selected for use in this study: one from a >90yo cognitively normal female (MADRC_2012, C1) and one from a 53yo female fAD patient carrying the PSEN1 L435F mutation (MADRC_2048, fAD1) (Table 1)(Oakley et al., 2020). Both patients underwent complete neuropathologic evaluation to confirm diagnosis and both were ApoE 3/3 genotype (Table 1).

Neuronal differentiation of iPSCs was performed utilizing stable lentiviral transduction with a puromycin-selectable Neurogenin2 (NGN2) construct combined with SMAD and WNT inhibition (Nehme et al., 2018; Oakley et al., 2020). We took advantage of this viral approach and co-infected Control and PSEN1 iPSCs with both the inducible NGN2 lentivirus and a second TauRD reporter lentivirus at the time of stable line generation. We reasoned that epigenetic events preventing silencing of the puromycin-selectable NGN2 lentivirus might also limit silencing of the co-infected TauRD reporter. This was indeed the case. Both resulting polyclonal NGN2/TauRD-YFP reporter iPSC lines expressed the TauRD-YFP reporter in a subset of cells for over 10 passages under puromycin selection without apparent decrease in expression level (Figure 1A, Extended Data Figure 1-1C, see methods). Both iPSC lines generated in this fashion also maintained a normal karyotype (Extended Data Figure 1-1 A-B). When measured by flow-cytometry, each iPSC-line expressed equivalent levels of the TauRD-YFP reporter in a similar percentage of iPSCs (Extended Data Figure 1-1C). After differentiation, YFP-expressing iPSC-neurons showed equivalent levels of reporter fluorescence between the two lines (Figure 1B and see below). Furthermore, neuronal cultures derived from the Control and PSEN1 TauRD reporter lines express equivalent levels of the TauRD-YFP reporter as compared to GAPDH on Western blot (Figure 1C). The percent of neuronal cells produced as measured by Tuj1 positivity was not significantly different between Control and PSEN1 mutant lines (Extended Data Figure 1-2 A, D). Prior studies show that the neurons produced by NGN2 induction in iPSCs are excitatory layer II/III cortical neurons (Zhang et al., 2013; Nehme et al., 2018). We confirmed this finding in our iPSC-neurons using immunohistochemistry for the upper-layer cortical markers Cux1 and Brn2, lower-layer

cortical marker Ctip2 (negative staining), and the glutamatergic neuron marker Tbr1 (Extended Data Figure 1-2 B, C, E).

Following the generation of NGN2/TauRD-YFP iPSCs from control and fAD lines, iPSC-neurons were produced and secreted levels of Aβ were measured. Consistent with prior results, neurons derived from the fAD PSEN1 L435F iPSC line produced significantly higher levels of Aβ43 species, and had higher Aβ43/40 and Aβ42/40 ratios, compared to control iPSC-neurons (Figure 1 D-E)(Oakley et al., 2020).

Tau seeding in Control and fAD human iPSC-derived neurons.

TauRD aggregation was induced in both Control and PSEN1 L435F mutant iPSC-neurons by adding phosphorylated tau “seeds” to the culture media. iPSC-neurons derived from both lines were exposed to brain lysate from mice overexpressing P301L mutant tau protein (rTg4510) and control littermates. The rTg4510 mice serve as a uniform, highly concentrated source of phosphorylated tau “seeds” that are taken up into neurons rapidly (within 24 hours) and induce aggregation of TauRD reporters(Takeda et al., 2015). Following treatment of iPSC-neurons with tau seeds in the absence of lipofectamine, TauRD reporter aggregates were observed to form within neurites and cell bodies in both cell lines within ~15 hours (Figure 2, Figure 3A). No spontaneous TauRD reporter aggregation was noted in neurons from either iPSC line (Figure 2) and has not been observed in cultures up to 6 months of age (data not shown). Control mouse brain lysate did not induce TauRD reporter aggregation (Figure 3A). Prior work has indicated that there may be templated misfolding and co-aggregation of endogenous tau species along with TauRD constructs (Reilly et al., 2017). To assess for this possibility, immunocytochemistry for endogenous phosphorylated tau was performed using an a phospho-tau-specific antibody that binds outside the TauRD domain present in the reporter (PHF1). PHF1 antibody demonstrated extremely weak, if any, PHF1 incorporation within TauRD aggregates at 7 days after seed exposure (Figure 2, inset).

TauRD aggregates formed only in a subset of neurons following exposure to seed material. To assess whether or not this cell-by-cell difference was reflective of variable seed uptake, fluorescently labeled rTg4510 lysate was applied to iPSC-neurons. Following a 5-day incubation to allow seeded TauRD aggregation, the neuronal uptake of fluorescent label (Alexa 647) was measured in the cytoplasmic and nuclear compartment of neurons with and without TauRD aggregates. We detected no difference in 647-label uptake between neurons with and without TauRD aggregates in either the cytoplasmic or nuclear compartments ($p=0.3$ for the neuronal soma as a whole, $p=0.19$ for the cytoplasmic compartment, and $p=0.89$ for the nuclear compartment) (Extended Data Figure 2-1). While these results suggest that there is no difference in brain lysate exposure between TauRD aggregating and non-aggregating cells, it is possible that more subtle, tau-specific uptake varies among cells.

In order to understand the time course of induced TauRD aggregation and its potential influence on neuronal survival, an in-vitro live-imaging assay was developed to monitor TauRD aggregate formation. Following addition of tau seeds, epifluorescent live-imaging was begun within 2 hours using a temperature and CO_2 controlled microscope (Cytation5, Biotek) with images taken every 2 hours for 7 days. A far-red nuclear dye (NucSpot 650, Biotium) was included in the media to allow time-lapse visualization of nuclear morphology and nuclear fragmentation associated with cell death. In iPSC-neurons, NucSpot 650 lightly labels the nuclei of living neurons and brightly labels nuclei following cell lysis. Beginning approximately 15 hours after seeding with rTg4510 lysate, we observe formation of TauRD aggregates in the soma and neurites of iPSC-neurons (Figure 3). These aggregates indicate neuronal uptake of misfolded tau and subsequent seeded reporter aggregation.

Live-imaging was performed on paired cultures of Control and PSEN1 TauRD-YFP expressing iPSC-neurons following the addition of varying concentrations of control and rTg4510 brain lysates. TauRD-YFP aggregates within neurites tended to be smaller than those that accumulate within cell bodies (Figure 2, Figure 3C-F). We took advantage of this difference to develop an automated quantification of TauRD-YFP aggregates within neurites (objects less than 4μm in size) (Extended Data Figure 3-1).

We then applied the automated quantification to Control and PSEN1 L435F neuronal cultures treated with control and seed-containing brain lysates over a range of concentrations (Figure 3A). Tau seed-containing brain lysate induced increasing numbers of TauRD-YFP aggregates over the course of 7 days when applied at concentrations of 1, 5 or 10 µg of total protein per well in a 96-well plate format (150µL media per well) (Figure 3A). Control brain lysates failed to induce TauRD-YFP aggregation under the same conditions (Figure 3A). Two-way ANOVA was then performed to evaluate the effect of cell line identity and rTg4510 brain lysate dosage on the area under the curve (AUC) depicted in Figure 3A (results of 1, 5 and 10 µg rTg4510 conditions). There was a significant effect of rTg4510 lysate dosage on AUC ($F(2, 18)=11.3$, $p=0.0007$), but not of cell line identity ($F(2, 18)=2.2$, $p=0.159$) and there was no significant interaction between cell line identity and lysate dosage ($F(2, 18)=0.11$, $p=0.90$) (Figure 3B). Pairwise comparisons of AUC as a function of lysate dosage for each line are depicted in Figure 3B. Percent Tuj1 positive cells and average neurite density were not significantly different between the Control and PSEN1 iPSC-neuron cultures at the end of live-imaging assays (Extended Data Figure 1-2 A, D, Extended Data Figure 3-2).

Following formation, aggregates are trafficked within neurites and growth cones and accumulate in cell bodies (Figure 3C-F, Movie 1). We observed that some aggregate-containing cells underwent nuclear fragmentation and cell death, highlighted by a large increase in fluorescence intensity of the far-red nuclear dye, and thus were also able to monitor the temporal relationship of aggregate formation and cell death in individual neurons (Figure 3 C-F, Movies 1-3).

fAD iPSC-neurons show accelerated tau seed formation.

Because fAD-causing mutations in PSEN1 are thought to accelerate the formation of age-related neurofibrillary tangles within neurons, we next sought to determine whether or not PSEN1 L435F neurons exhibited differences in the profile of TauRD-YFP seed formation in the live-imaging assay (Oddo et al., 2003; Sperling RA et al., 2014). Measurement of seed formation in neurites indicates that there is a non-significant trend towards more TauRD neurite seeds in the PSEN1 L435F cell line

(Figure 3). In cultures treated with the highest dose of seed-material, there was an apparent early acceleration of seed formation in neurites 24-48 hours after seed addition, with a significantly higher slope of the seeding curve between these timepoints in PSEN1 mutant cells compared to Control ($p=0.016$). Differences in the slope of seeding were not seen in conditions with lower concentrations of seed material and they were not present at later time points in the assay.

To extend this analysis, single-neuron tracking macros were developed for NIH ImageJ to facilitate manual longitudinal phenotyping of individual cells throughout the course of live imaging experiments (Extended Data Figure 4-1). Using this software, all individually identifiable YFP-positive cells with neuronal morphology in the high-dose seed condition were tracked and the presence of TauRD-YFP aggregates in the cell soma was evaluated per-timepoint (n=1598 Control neurons and n=983 PSEN1 neurons from 4 independent neuronal differentiations). Cell death was highlighted using a far-red nuclear dye (NucSpot 650) and recorded when present (Movies 2 & 3). Neurons that left the field of view during the course of the experiment were classified as censored at that timepoint for the purpose of subsequent data analysis.

Single cell tracking revealed accelerated cell soma TauRD-YFP aggregate formation in PSEN1 mutant iPSC-neurons treated with tau seeds compared to control. 48 hours after seed-material addition, a greater percentage of PSEN1 mutant neurons contained cell soma aggregates compared to controls (34.4% +/- 3.8 s.d. in PSEN1 vs. 17.4%+/-4.1 s.d. in Control neurons $p=0.0009$) (Figure 4A). A higher percentage of soma aggregate-containing neurons was also observed in PSEN1 mutant neurons at the endpoint of the 7-day experiment (64.3% +/- 7.7 s.d in PSEN1 vs 49.7%+/-4.3 s.d. in Control neurons $p=0.023$) (Figure 4A). The overall number of neurons counted was not significantly different between the two lines ($p=0.129$). Furthermore, cumulative event analysis showed that cell soma aggregation tended to occur earlier in PSEN1 mutant neurons compared to Control ($p<0.001$) (Figure 4B).

Because it is possible that subtle variation in the expression level of the TauRD reporter might underly a portion of the observed differences between Control and PSEN1 neurons in this assay, we then

382 measured the average reporter fluorescence intensity in neuronal somas at the beginning of the assay
383 (t0) and correlated this with the subsequent onset of TauRD reporter aggregation on a per-cell basis
384 (Figure 4C). There was no significant difference in the average t0 neuronal soma fluorescence intensity
385 between the two cell lines (average PSEN1/Control ratio = 0.88 +/- 0.08 s.d. p=0.082, n=3).
386 Additionally, there was no relationship between TauRD reporter expression and onset of reporter
387 aggregation in either the Control or PSEN1 cell lines (Control R^2=-0.032, p=0.44, PSEN1 R^2=-0.042,
388 p=0.38) (Figure 4C).

389 Neuronal cell death follows tau seed formation in both Control and fAD iPSC-neurons.

390 The aggregate formation and neuronal survival data generated above was then used to produce
391 Kaplan-Meier survival probability curves comparing neurons with and without aggregates under
392 identical conditions in the same well. These data demonstrate that cell soma aggregate formation is
393 associated with an increased risk of subsequent cell death. Since any TauRD-aggregate-mediated
394 neuronal death may be a time-dependent phenomenon, survival analysis was first performed on early
395 aggregate-forming neurons, which would subsequently have the longest exposure to intracellular
396 TauRD aggregates. In both Control and PSEN1 cells, neurons that develop cell soma aggregates
397 within 48 hours of exposure to seed material are at a higher risk of subsequent death compared to all
398 other neurons that have not yet developed aggregates at 48 hours (n=4, p<0.0001) (Figure 5 A-B).
399 Similar results were also present for comparisons between the groups of neurons that developed
400 aggregates at any time and those that remained aggregate-free throughout the experiment (p=0.041 for
401 control and p<0.0001 for PSEN1). These results indicate a deleterious effect of tau “seed” uptake
402 followed by aggregation, as well as a delay between aggregation and death. At the time of cell death,
403 fragmentation of the neuronal nucleus occurs along with lysis of the cell (Figure 3 C-F, Movies 1-3).
404 Furthermore, there was a very weak positive correlation between TauRD fluorescence intensity and cell
405 survival, present only in control cells, suggesting that expression level of mutant TauRD was not a

406 driving factor in neuronal cell death (Control R^2=0.18, p=0.044, PSEN1 R^2=0.031, p=0.72) (Extended
407 Data Figure 5-1).

408 Although the PSEN1 mutant iPSC-neurons demonstrated accelerated aggregate formation, there was
409 no difference in neuronal survival between the two cell lines after TauRD aggregation. Survival of
410 Control and PSEN1 early aggregate forming neurons was not significantly different (p=0.12) (Figure
411 5C). As a group, PSEN1 neurons that developed aggregates at any time during the experiment did
412 show a reduced survival compared to Control neurons in the same category (p=0.0038) (Extended
413 Data Figure 5-2). However, a separate analysis of post-aggregate survival time for all aggregate-
414 forming neurons showed no significant difference between the Control and PSEN1 cell lines (p=0.22)
415 (Figure 5D).These results suggest that reduced survival in the PSEN1 line on average is caused by
416 accelerated aggregate formation and not a change in post-aggregate survival. A Cox proportional
417 hazard model supports this notion. While the hazard ratio for cell death was significantly lower in cells
418 that had not developed aggregates by 48 hours compared to those that had, there was no contribution
419 of cell line identity to hazard for cell death (Extended Data Figure 5-3). These findings highlight the
420 importance of using single cell longitudinal analyses to decouple the rate of aggregate formation from
421 subsequent neuronal phenotypes.

422 Morphologic tau strains show differential toxicity and propagation.

423 Prior studies indicate that multiple morphologic “strains” of tau can be identified and propagated as
424 TauRD aggregates in HEK cells (Sanders et al., 2014). We assessed a random sample of tracked
425 neurons across 4 biological replicates (n=381 control, n=311 PSEN1 cells) and assigned strain
426 morphologies where possible while blinded to cell line and survival status (n=322 control neurons,
427 n=267 PSEN1 neurons). Two main morphologic strains or patterns were present in iPSC-neurons: 1)
428 “ordered” aggregates characterized by one or more large cytoplasmic condensations of TauRD, often
429 with compaction over time, and 2) “disordered” aggregates, with many small cytoplasmic puncta that
430 failed to coalesce during the imaging period (Figure 6A). Rarely, iPSC-neurons demonstrated

prominent nuclear speckling of TauRD aggregates or a cytoplasmic aggregation pattern that did not fit into the above categories, sometimes characterized by a lenticular morphology (Figure 6A). Surprisingly, the relative frequencies of ordered and disordered TauRD aggregates differed between the control and PSEN1 lines, with a shift towards more ordered aggregates in PSEN1 mutant neurons (between line frequency comparisons: p=0.009 for disordered aggregates and p=0.024 for ordered aggregates) (Figure 6B). Among the classes of aggregates identified, there were no cell-line-dependent differences in neuronal lifespan (Figure 6C). However, cells with ordered TauRD aggregates had a reduced lifespan compared to those with disordered aggregates (p=1e-05 for Control neurons and p=0.0008 for PSEN1 neurons) (Figure 6D). This result suggests that aggregate strain morphology may play a role in tau toxicity or reflect a variable degree of exposure to toxic tau species. Interestingly, ordered TauRD aggregates began earlier during the course of experiments than those that were disordered (p=0.054 for Control neurons and p=0.023 for PSEN1 neurons) (Figure 6E). Because it is possible that ordered aggregate morphologies represent the evolution of disordered aggregates over time, we assessed the amount of time that each aggregate was observed. There was no significant difference in this metric between the ordered and disordered morphologies (“aggregate lifespan”, p=0.9 for Control neurons and p=0.21 for PSEN1 neurons) (Figure 6F). Thus, our results are consistent with strain-differences in TauRD aggregates that represent an interaction between cell line and exogenous tau species and subsequently influence neuronal survival.

Discussion:

This work establishes real-time assessment of tau aggregation and subsequent neuronal survival in human iPSC-neurons derived from patients with neurodegenerative disease. We have developed a live imaging protocol that facilitates bulk quantification of TauRD reporter aggregation as well as longitudinal assessment of aggregation and neuronal death at single-cell resolution. Our implementation of a custom single-neuron tracking workflow results in a simple yet robust method for phenotyping individual cells throughout the course of experiments and allows censoring of neurons that

leave the field of view or become otherwise obscured. Commercial equipment and an open source custom software simplify the acquisition and evaluation of the images and provide a robust technology for 4D analyses. These data are used to generate Kaplan-Meier survival probability curves comparing neurons with and without TauRD aggregates under identical conditions in the same well. We are then able to compare the survival of iPSC-neurons derived from multiple patients, correcting for differences in the rate of TauRD aggregation.

We observed neurotoxicity following treatment with tau seeds in both control and PSEN1 L435F iPSC-neurons. Neurons that aggregated the TauRD reporter were significantly more likely to undergo cell death during the course of the experiment compared to neurons in the same well that did not show TauRD aggregation. These results indicate a deleterious effect of tau uptake followed by reporter aggregation, as well as a delay between aggregation and death. To our knowledge, this is the first study to directly visualize tau aggregation and subsequent neuronal cell death from start to finish in single human neurons.

Neuronal death in our system is accelerated compared to that seen in human patients or *in vivo* in tangle-bearing MAPT mutant mouse models (de Calignon et al., 2010). Furthermore, acute toxicity was not present in mouse primary neurons treated with the seed-competent fraction of rTg4510 brain lysate (Takeda et al., 2015). This suggests that the observed rate of cell death in iPSC-neurons may be increased by an interaction between soluble tau oligomer species and TauRD aggregation (Lasagna-Reeves et al., 2010; Ghag et al., 2018). Our group's prior work measuring tau toxicity in primary neurons was performed using population averages (Takeda et al., 2015). Applying longitudinal single neuron survival analysis to this model may reveal more subtle tau-dependent neuronal cell death.

The absence of glia in these iPSC-neuron cultures may also influence neuronal susceptibility to tau toxicity. Astrocytes, for instance, support the maturation and connectivity of neurons grown in culture (Molofsky et al., 2012; Nehme et al., 2018), and secrete neurotrophic factors that may have activity beyond those already present in the media formulation (Verkhratsky et al., 2016). However, astrocytes

481 are a heterogenous class of cells that can undergo reactive transformations, both in-vitro and in-vivo,
482 and this may also influence their effects on neuronal survival (Roybon et al., 2013; Khakh and
483 Sofroniew, 2015). Additionally, both astrocytes (Martini-Stoica et al., 2018; Perea et al., 2019; Kovacs,
484 2020) and microglia (Hopp et al., 2018) take up and metabolize tau in cell culture models and in some
485 cases may release bioactive tau fragments back into the culture media. Studying the interplay between
486 neurotrophic factor support and glial-dependent tau processing could be a fruitful avenue of further
487 research approached using primary or iPS-derived glia and a combination of co-culture and conditioned
488 media preparations.

489 In this study, survival in TauRD aggregate-bearing neurons is compared to adjacent neurons in the
490 same dish as an attempt to control for overall exposure to potentially toxic soluble tau oligomers and
491 other non-cell-autonomous factors. Prior work with rTg4510 brain lysates shows that uptake into
492 neurons occurs within 24 hours; well before the observed differences in survival between aggregate-
493 bearing and aggregate-free neurons (Takeda et al., 2015). Still, it seems possible that cell-by-cell
494 differences in the rate of tau uptake could contribute to variability seen in the onset of TauRD
495 aggregation. However, experiments with labeled seed-containing brain lysates failed to establish a
496 relationship between bulk lysate uptake and TauRD aggregation. Moreover, we found no correlation
497 between TauRD expression and the onset of TauRD aggregation and a weak positive correlation
498 between TauRD expression and survival in Control iPSC-neurons. These results suggest that tau
499 seeding in iPSC-neurons may be modulated by other homeostatic mechanisms and that these
500 mechanisms may be activated at variable levels amongst adjacent neurons.

501 Important future directions will include elucidating the mechanism(s) of tau uptake and cell death in
502 seed-containing iPSC-neurons. Apoptotic neuronal death is believed to occur in AD and has been
503 directly observed in animal models of AD and other tauopathies(Wirths and Bayer, 2010; Serrano-Pozo
504 et al., 2011). However, the downstream effectors of neuronal tau toxicity *in vitro* are not well
505 established. In addition, understanding the pathways involved in tau uptake is an essential component

of future work, particularly in the context of recent reports identifying LRP1 as a ligand for tau internalization in human iPSCs (Evans et al., 2018; Rauch et al., 2020).

Our results show accelerated TauRD aggregation after seeding in iPSC-neurons containing the PSEN1 L435F mutation compared to control. An increased rate of TauRD reporter aggregation was present when measured both in the neurites and cell bodies of PSEN1 L435F iPSC-neurons. Spontaneous tau aggregation is not a general feature of AD iPSC-neuron models and was not seen in PSEN1 L435F iPSC-neurons (Sproul, 2015; Mungenast et al., 2016; Oakley et al., 2020). However, there was no difference in post-aggregate survival time between PSEN1 and Control iPSC-neurons, suggesting that the rate an aggregate forms is a kinetic choke point – possibly a time limiting feature of tau induced cytotoxicity. In accord with this interpretation, a Cox-proportional hazard model identified aggregation exposure time, but not PSEN1 mutation, as a significant contributor to overall neuronal survival.

These findings support a model where alterations in PSEN1 activity function upstream of tau aggregate formation in the pathogenesis of tau-induced neurotoxicity. In such a model, increased levels of longer Aβ species caused by mutations in PSEN1 would lead to increased tau phosphorylation which, in turn, would increase the rate of tau aggregation. Subsequent to tau aggregation, neuronal cell death would proceed by Aβ-independent mechanisms. Because this model posits that tau aggregation is the key insult that drives neuronal death, one would expect the post-tau-aggregation rate of neuronal death to be equivalent between PSEN1 mutation-driven and sporadic causes of tau aggregation. This idea is consistent with numerous pieces of genetic and experimental data in Alzheimer disease. Indeed, as is shown in our previous work as well as this publication, PSEN1 L435F iPSC-neurons produce elevated levels of Aβ43 species and higher Aβ43/40 and Aβ42/40 ratios, indicating a potential cause of elevated seeding (Oakley et al., 2020).

We did not observe substantial incorporation of endogenous PHF-1 phosphorylated tau species into TauRD reporter aggregates. Qualitatively, this finding concurs with prior literature on TauRD aggregates, which have been shown to incorporate only small amounts of endogenous tau, sometimes

apparent only by Immuno-EM(Reilly et al., 2017). While endogenous tau is not necessary for propagation of misfolded tau species between neurons, it is thought to play a role in downstream neurotoxicity in mouse models(Wegmann et al., 2015). Additionally, the iPSC-neurons used in this work express predominantly 3R tau isoforms at day 28 by Western blot (Oakley et al., 2020). This may influence the incorporation of endogenous tau into reporter aggregates, which are homologous to 4R tau.

In accord with prior studies using TauRD reporters in HEK cells, we identified several morphologic strains of aggregates that formed in response to tau seeds (Sanders et al., 2014; Kaufman et al., 2016; Kaufman et al., 2017). To our knowledge, this phenomenon has not yet been reported in human neurons. The specific TauRD aggregate morphologies identified in iPSCs are roughly equivalent to those seen in HEK cells and largely fell into categories of “Ordered” or “Disordered”. Interestingly, we found that “Ordered” aggregates were associated with reduced neuronal survival compared to “Disordered” aggregates and occurred more frequently in the PSEN1 L435F line than control. These findings suggest that strain- and patient-specific differences in tau propagation could be studied using this approach. Because we used a homogeneous preparation from a transgenic animal as the source of tau seeds, our results suggest that multiple strains of seed-competent tau may exist contemporaneously in the same preparation, and potentially even in the same brain. Future work could assess whether specific morphologic strains of tau are present at differential rates in donated brain human tissues from different AD patients. Recent work from our lab and others demonstrates that there is a large degree of heterogeneity of p-tau profile and tau seeding activity among AD patients (Holmes et al., 2014; Dujardin et al., 2020). It would be intriguing to ask whether this variability also translates into changes in tau aggregate morphology using a large panel of well characterized reference brain tissues.

The use of patient-derived iPSC lines as a source of human neurons will allow future exploration of patient-specific influences on neuronal tau seeding and survival. Given the wide range of Aβ plaque

and tau tangle burden present in AD patients at autopsy (Braak et al., 2011; Kapasi et al., 2017), it will be informative to expand this technique across multiple sporadic and familial AD donors and to test the hypothesis that various genetic risk factors or specific phenotypes observed at autopsy reflect an endogenous propensity to tau aggregation in neuronal cells. Additionally, the ability to quantitively measure tau seed uptake and aggregation in human neurons should have utility in drug-screening and mechanistic studies focused on tau propagation in neurodegenerative disease.

Ultimately, this work demonstrates a tau seeding phenomenon in human iPSC-neurons that is coupled with downstream neuronal death. Following seeding with brain lysates from mice overexpressing human P301L mutant tau, TauRD-YFP aggregation was associated with reduced neuronal survival in both Control and PSEN1 L435 mutant iPSC-neurons. TauRD reporter aggregation occurred more rapidly in the PSEN1 L435F line, in accord with our earlier observations that these cells accumulate phospho-tau at baseline (Oakley et al., 2020). These findings were established using cell-by-cell comparison between neurons in the same well that did or did not aggregate the TauRD reporter. Furthermore, specific morphologies of TauRD aggregation were associated with increased neurotoxicity. The development of this methodology, along with the current results, suggests ways of investigating differences in tau toxicity in different tauopathies, and even among individual patients with sporadic AD.

Author Contributions: D.H.O., B.T.H., and M.P.F. designed all experiments and subsequent analyses. S.D. and R.E.B. assisted in experimental design and development of key reagents. D.H.O., N.K., M.C., and C.C. carried out all experiments. D.H.O. performed data analysis and manuscript preparation.

Funding: D.H.O. is a recipient of an Alzheimer's Association Clinician Scientist Fellowship (2018-AASCF-592307) and a Jack Satter Foundation Award. D.H.O. is partially supported by the Dr. and Mrs. E. P. Richardson, Jr Fund for Neuropathology at MGH. The Massachusetts Alzheimer's Disease Research Center is supported by the National Institute on Aging NIA (Grant P30AG062421). The Cure Alzheimer Fund and NIH grant 1R01AG058002-01 supported the establishment of the cell lines used. S.D. is supported by the Alzheimer's association (2018-AARF-591935) and the Martin L. and Sylvia Seevak Hoffman Fellowship for Alzheimer's Research.

ORCIDs: 0000-0002-6998-9510 (D.H.O.), 0000-0002-1405-4590 (N.K.), 0000-0002-4033-7930 (M.C.), 0000-0002-5614-341X (S.D.), 0000-0001-9640-0575 (R.E.B.), 0000-0002-7959-9401 (B.T.H.), 0000-0002-3940-9861 (M.P.F.)

Keywords: iPSC, MAPT, Alzheimer Disease, FTLD, Tau Seeding, Tau Aggregation, Neurotoxicity, PSEN1 L435F

References:

Arriagada PV, Growdon JH, Hedley-Whyte ET, Hyman BT (1992) Neurofibrillary tangles but not senile plaques parallel duration and severity of Alzheimer's disease. Neurology 42:631-639.

Bennett RE, DeVos SL, Dujardin S, Corjuc B, Gor R, Gonzalez J, Roe AD, Frosch MP, Pitstick R, Carlson GA, Hyman BT (2017) Enhanced Tau Aggregation in the Presence of Amyloid beta. Am J Pathol 187:1601-1612.

Braak H, Thal DR, Ghebremedhin E, Del Tredici K (2011) Stages of the pathologic process in Alzheimer disease: age categories from 1 to 100 years. J Neuropathol Exp Neurol 70:960-969.

Brier MR, Gordon B, Friedrichsen K, McCarthy J, Stern A, Christensen J, Owen C, Aldea P, Su Y, Hassenstab J, Cairns NJ, Holtzman DM, Fagan AM, Morris JC, Benzinger TL, Ances BM (2016) Tau and Abeta imaging, CSF measures, and cognition in Alzheimer's disease. Sci Transl Med 8:338ra366.

Choi SH, Kim YH, Hebisch M, Sliwinski C, Lee S, D'Avanzo C, Chen H, Hooli B, Asselin C, Muffat J, Klee JB, Zhang C, Wainger BJ, Peitz M, Kovacs DM, Woolf CJ, Wagner SL, Tanzi RE, Kim DY (2014) A three-dimensional human neural cell culture model of Alzheimer's disease. Nature 515:274-278.

de Calignon A, Fox LM, Pitstick R, Carlson GA, Bacskai BJ, Spires-Jones TL, Hyman BT (2010) Caspase activation precedes and leads to tangles. Nature 464:1201-1204.

DeVos SL, Corjuc BT, Oakley DH, Nobuhara CK, Bannon RN, Chase A, Commins C, Gonzalez JA, Dooley PM, Frosch MP, Hyman BT (2018) Synaptic Tau Seeding Precedes Tau Pathology in Human Alzheimer's Disease Brain. Front Neurosci 12:267.

DeVos SL, Miller RL, Schoch KM, Holmes BB, Kebodeaux CS, Wegener AJ, Chen G, Shen T, Tran H, Nichols B, Zanardi TA, Kordasiewicz HB, Swayze EE, Bennett CF, Diamond MI, Miller TM (2017) Tau reduction prevents neuronal loss and reverses pathological tau deposition and seeding in mice with tauopathy. Sci Transl Med 9.

Dujardin S, Lecolle K, Caillierez R, Begard S, Zommer N, Lachaud C, Carrier S, Dufour N, Auregan G, Winderickx J, Hantraye P, Deglon N, Colin M, Buee L (2014) Neuron-to-neuron wild-type Tau protein transfer through a trans-synaptic mechanism: relevance to sporadic tauopathies. Acta Neuropathol Commun 2:14.

Dujardin S et al. (2020) Tau molecular diversity contributes to clinical heterogeneity in Alzheimer's disease. Nat Med.

Evans LD, Wassmer T, Fraser G, Smith J, Perkinton M, Billinton A, Livesey FJ (2018) Extracellular Monomeric and Aggregated Tau Efficiently Enter Human Neurons through Overlapping but Distinct Pathways. Cell Rep 22:3612-3624.

Furman JL, Vaquer-Alicea J, White CL, 3rd, Cairns NJ, Nelson PT, Diamond MI (2017) Widespread tau seeding activity at early Braak stages. Acta Neuropathol 133:91-100.

Ghag G, Bhatt N, Cantu DV, Guerrero-Munoz MJ, Ellsworth A, Sengupta U, Kayed R (2018) Soluble tau aggregates, not large fibrils, are the toxic species that display seeding and cross-seeding behavior. Protein Sci 27:1901-1909.

He Z, Guo JL, McBride JD, Narasimhan S, Kim H, Changolkar L, Zhang B, Gathagan RJ, Yue C, Dengler C, Stieber A, Nitla M, Coulter DA, Abel T, Brunden KR, Trojanowski JQ, Lee VM (2018) Amyloid-beta plaques enhance Alzheimer's brain tau-seeded pathologies by facilitating neuritic plaque tau aggregation. Nat Med 24:29-38.

Holmes BB, Furman JL, Mahan TE, Yamasaki TR, Mirbaha H, Eades WC, Belaygorod L, Cairns NJ, Holtzman DM, Diamond MI (2014) Proteopathic tau seeding predicts tauopathy in vivo. Proc Natl Acad Sci U S A 111:E4376-4385.

Hopp SC, Lin Y, Oakley D, Roe AD, DeVos SL, Hanlon D, Hyman BT (2018) The role of microglia in processing and spreading of bioactive tau seeds in Alzheimer's disease. J Neuroinflammation 15:269.

Hyman BT, Phelps CH, Beach TG, Bigio EH, Cairns NJ, Carrillo MC, Dickson DW, Duyckaerts C, Frosch MP, Masliah E, Mirra SS, Nelson PT, Schneider JA, Thal DR, Thies B, Trojanowski JQ, Vinters HV, Montine TJ (2012)

National Institute on Aging-Alzheimer's Association guidelines for the neuropathologic assessment of Alzheimer's disease. Alzheimer's Dementia J Alzheimer's Assoc 8:1-13.

Kapasi A, DeCarli C, Schneider JA (2017) Impact of multiple pathologies on the threshold for clinically overt dementia. Acta Neuropathol 134:171-186.

Kaufman SK, Thomas TL, Del Tredici K, Braak H, Diamond MI (2017) Characterization of tau prion seeding activity and strains from formaldehyde-fixed tissue. Acta Neuropathol Commun 5:41.

Kaufman SK, Sanders DW, Thomas TL, Ruchinskas AJ, Vaquer-Alicea J, Sharma AM, Miller TM, Diamond MI (2016) Tau Prion Strains Dictate Patterns of Cell Pathology, Progression Rate, and Regional Vulnerability In Vivo. Neuron 92:796-812.

Khakh BS, Sofroniew MV (2015) Diversity of astrocyte functions and phenotypes in neural circuits. Nat Neurosci 18:942-952.

Komatsubara AT, Matsuda M, Aoki K (2015) Quantitative analysis of recombination between YFP and CFP genes of FRET biosensors introduced by lentiviral or retroviral gene transfer. Sci Rep 5:13283.

Kovacs GG (2020) Astroglia and Tau: New Perspectives. Front Aging Neurosci 12:96.

Lasagna-Reeves CA, Castillo-Carranza DL, Guerrero-Muoz MJ, Jackson GR, Kayed R (2010) Preparation and characterization of neurotoxic tau oligomers. Biochemistry 49:10039-10041.

Martini-Stoica H, Cole AL, Swartzlander DB, Chen F, Wan YW, Bajaj L, Bader DA, Lee VMY, Trojanowski JQ, Liu Z, Sardiello M, Zheng H (2018) TFEB enhances astroglial uptake of extracellular tau species and reduces tau spreading. J Exp Med 215:2355-2377.

Molofsky AV, Krencik R, Ullian EM, Tsai HH, Deneen B, Richardson WD, Barres BA, Rowitch DH (2012) Astrocytes and disease: a neurodevelopmental perspective. Genes Dev 26:891-907.

Mudher A, Colin M, Dujardin S, Medina M, Dewachter I, Alavi Naini SM, Mandelkow EM, Mandelkow E, Buee L, Goedert M, Brion JP (2017) What is the evidence that tau pathology spreads through prion-like propagation? Acta Neuropathol Commun 5:99.

Mungenast AE, Siegert S, Tsai LH (2016) Modeling Alzheimer's disease with human induced pluripotent stem (iPS) cells. Mol Cell Neurosci 73:13-31.

Nehme R et al. (2018) Combining NGN2 Programming with Developmental Patterning Generates Human Excitatory Neurons with NMDAR-Mediated Synaptic Transmission. Cell Rep 23:2509-2523.

Nelson PT et al. (2012) Correlation of Alzheimer disease neuropathologic changes with cognitive status: a review of the literature. J Neuropathol Exp Neurol 71:362-381.

Nicholls SB, DeVos SL, Commins C, Nobuhara C, Bennett RE, Corjuc DL, Maury E, Eftekharzadeh B, Akingbade O, Fan Z, Roe AD, Takeda S, Wegmann S, Hyman BT (2017) Characterization of TauC3 antibody and demonstration of its potential to block tau propagation. PLoS One 12:e0177914.

Nobuhara CK et al. (2017) Tau Antibody Targeting Pathological Species Blocks Neuronal Uptake and Interneuron Propagation of Tau in Vitro. Am J Pathol 187:1399-1412.

Oakley DH, Chung M, Klickstein N, Commins C, Hyman BT, Frosch MP (2020) The Alzheimer Disease-Causing Presenilin-1 L435F Mutation Causes Increased Production of Soluble Abeta43 Species in Patient-Derived iPSC-Neurons, Closely Mimicking Matched Patient Brain Tissue. J Neuropathol Exp Neurol.

Oddo S, Caccamo A, Shepherd JD, Murphy MP, Golde TE, Kayed R, Metherate R, Mattson MP, Akbari Y, LaFerla FM (2003) Triple-transgenic model of Alzheimer's disease with plaques and tangles: intracellular Abeta and synaptic dysfunction. Neuron 39:409-421.

Perea JR, Lopez E, Diez-Ballesteros JC, Avila J, Hernandez F, Bolos M (2019) Extracellular Monomeric Tau Is Internalized by Astrocytes. Front Neurosci 13:442.

Ramsden M, Kotilinek L, Forster C, Paulson J, McGowan E, SantaCruz K, Guimaraes A, Yue M, Lewis J, Carlson G, Hutton M, Ashe KH (2005) Age-dependent neurofibrillary tangle formation, neuron loss, and memory impairment in a mouse model of human tauopathy (P301L). J Neurosci 25:10637-10647.

683 Rauch JN, Luna G, Guzman E, Audouard M, Challis C, Sibih YE, Leshuk C, Hernandez I, Wegmann S, Hyman BT,
684 Gradinaru V, Kampmann M, Kosik KS (2020) LRP1 is a master regulator of tau uptake and spread.
685 Nature.
686 Reilly P, Winston CN, Baron KR, Trejo M, Rockenstein EM, Akers JC, Kfoury N, Diamond M, Masliah E, Rissman
687 RA, Yuan SH (2017) Novel human neuronal tau model exhibiting neurofibrillary tangles and transcellular
688 propagation. Neurobiol Dis 106:222-234.
689 Roybon L, Lamas NJ, Garcia AD, Yang EJ, Sattler R, Lewis VJ, Kim YA, Kachel CA, Rothstein JD, Przedborski S,
690 Wichterle H, Henderson CE (2013) Human stem cell-derived spinal cord astrocytes with defined mature
691 or reactive phenotypes. Cell Rep 4:1035-1048.
692 Sanders DW, Kaufman SK, DeVos SL, Sharma AM, Mirbaha H, Li A, Barker SJ, Foley AC, Thorpe JR, Serpell LC,
693 Miller TM, Grinberg LT, Seeley WW, Diamond MI (2014) Distinct tau prion strains propagate in cells and
694 mice and define different tauopathies. Neuron 82:1271-1288.
695 Santacruz K, Lewis J, Spires T, Paulson J, Kotilinek L, Ingelsson M, Guimaraes A, DeTure M, Ramsden M,
696 McGowan E, Forster C, Yue M, Orne J, Janus C, Mariash A, Kuskowski M, Hyman B, Hutton M, Ashe KH
697 (2005) Tau suppression in a neurodegenerative mouse model improves memory function. Science
698 309:476-481.
699 Serrano-Pozo A, Frosch MP, Masliah E, Hyman BT (2011) Neuropathological alterations in Alzheimer disease.
700 Cold Spring Harb Perspect Med 1:a006189.
701 Sperling RA, Rentz DM, Johnson KA, Karlawish J, Donohue M, Salmon DP, P A (2014) The A4 Study: Stopping AD
702 Before Symptoms Begin? Science Translational Medicine 6:228fs213-228fs213.
703 Sproul AA (2015) Being human: The role of pluripotent stem cells in regenerative medicine and humanizing
704 Alzheimer's disease models. Mol Aspects Med 43-44:54-65.
705 Takeda S, Wegmann S, Cho H, DeVos SL, Commins C, Roe AD, Nicholls SB, Carlson GA, Pitstick R, Nobuhara CK,
706 Costantino I, Frosch MP, Muller DJ, Irimia D, Hyman BT (2015) Neuronal uptake and propagation of a
707 rare phosphorylated high-molecular-weight tau derived from Alzheimer's disease brain. Nat Commun
708 6:8490.
709 Takeda S, Commins C, DeVos SL, Nobuhara CK, Wegmann S, Roe AD, Costantino I, Fan Z, Nicholls SB, Sherman
710 AE, Trisini Lipsanopoulos AT, Scherzer CR, Carlson GA, Pitstick R, Peskind ER, Raskind MA, Li G, Montine
711 TJ, Frosch MP, Hyman BT (2016) Seed-competent high-molecular-weight tau species accumulates in the
712 cerebrospinal fluid of Alzheimer's disease mouse model and human patients. Ann Neurol 80:355-367.
713 Verkhratsky A, Matteoli M, Parpura V, Mothet JP, Zorec R (2016) Astrocytes as secretory cells of the central
714 nervous system: idiosyncrasies of vesicular secretion. EMBO J 35:239-257.
715 Wegmann S, Maury EA, Kirk MJ, Saqran L, Roe A, DeVos SL, Nicholls S, Fan Z, Takeda S, Cagsal-Getkin O, William
716 CM, Spires-Jones TL, Pitstick R, Carlson GA, Pooler AM, Hyman BT (2015) Removing endogenous tau
717 does not prevent tau propagation yet reduces its neurotoxicity. EMBO J 34:3028-3041.
718 Wirths O, Bayer TA (2010) Neuron loss in transgenic mouse models of Alzheimer's disease. Int J Alzheimers Dis
719 2010.
720 Zhang Y, Pak C, Han Y, Ahlenius H, Zhang Z, Chanda S, Marro S, Patzke C, Acuna C, Covy J, Xu W, Yang N, Danko T,
721 Chen L, Wernig M, Sudhof TC (2013) Rapid single-step induction of functional neurons from human
722 pluripotent stem cells. Neuron 78:785-798.

723

724

Figures and Tables:

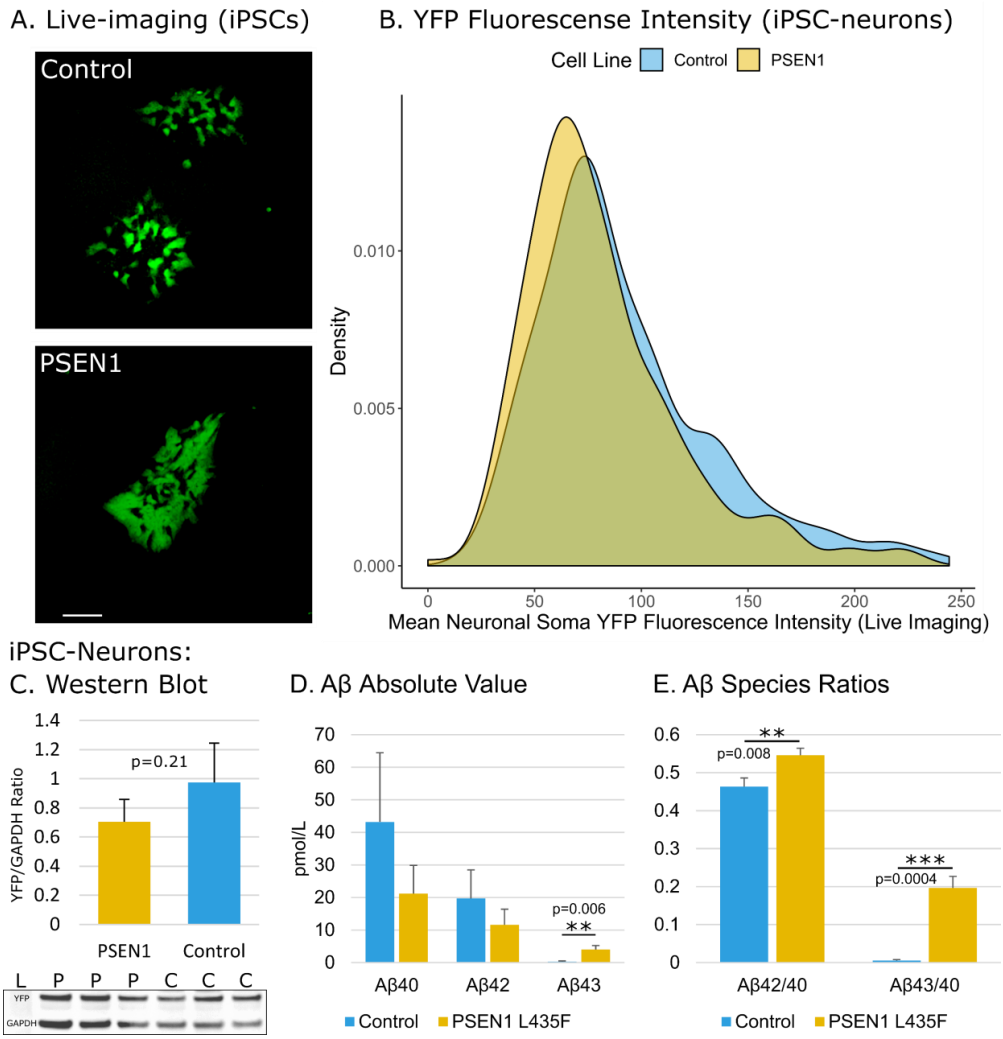

Fig 1: TauRD-YFP reporter and Aβ expression. A) Unstained fluorescent image of Control and PSEN1 iPSC colonies showing partial expression of TauRD reporter. Scale bar = 100 µm. B) Density distribution of neuronal soma YFP fluorescence intensity measured by live-imaging of iPSC-neurons at the end of differentiation (Day 15) Control=255 YFP-positive neurons, PSEN1=228 YFP-positive neurons. This analysis includes all YFP-expressing neurons visible on epifluorescent imaging. C) Western blot results demonstrating equivalent expression of the TauRD-YFP construct in PSEN1 L435F and Control iPSC-derived neuronal cultures (n=3 independent neuronal differentiations, day 28, +/- s.d.). D-E) Secreted Aβ43 species and Aβ42/40, Aβ43/40, ratios are elevated in PSEN1 L435F iPSC-neurons (+/- s.d.). D) Absolute Aβ levels in media for Control and PSEN1 mutant iPSC-neurons (D28 media, ELISA, +/- s.d.). E) Aβ42 and Aβ43 to Aβ40 ratios (+/- s.d.). See Extended Data Figures 1-1 & 1-2.

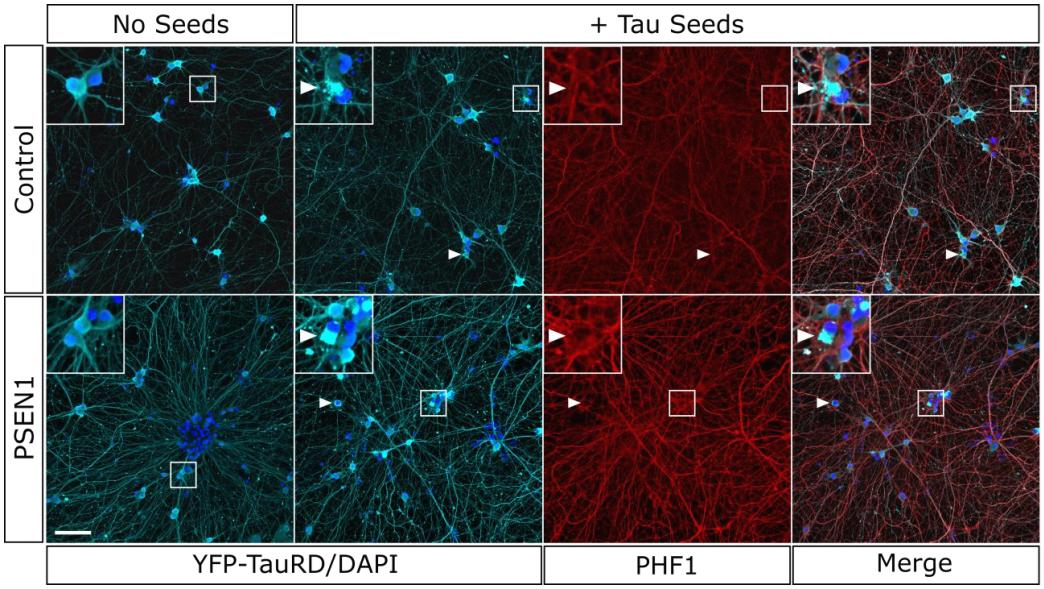

Fig 2: TauRD-YFP reporter expression in iPSC-neurons and aggregation in response to misfolded tau seeds. Control and PSEN1 mutant iPSC-neurons as indicated with and without exposure to tau seeds for 7 days prior to fixation and immunohistochemistry for DAPI (blue), YFP (cyan), and phospho-tau (PHF1, red). Following exposure to tau seeds, iPSC-neurons develop aggregates of TauRD-YFP reporter (arrowheads), shown at higher magnification in inset. Scale bar = 50µM. See Extended Data Figure 2-1.

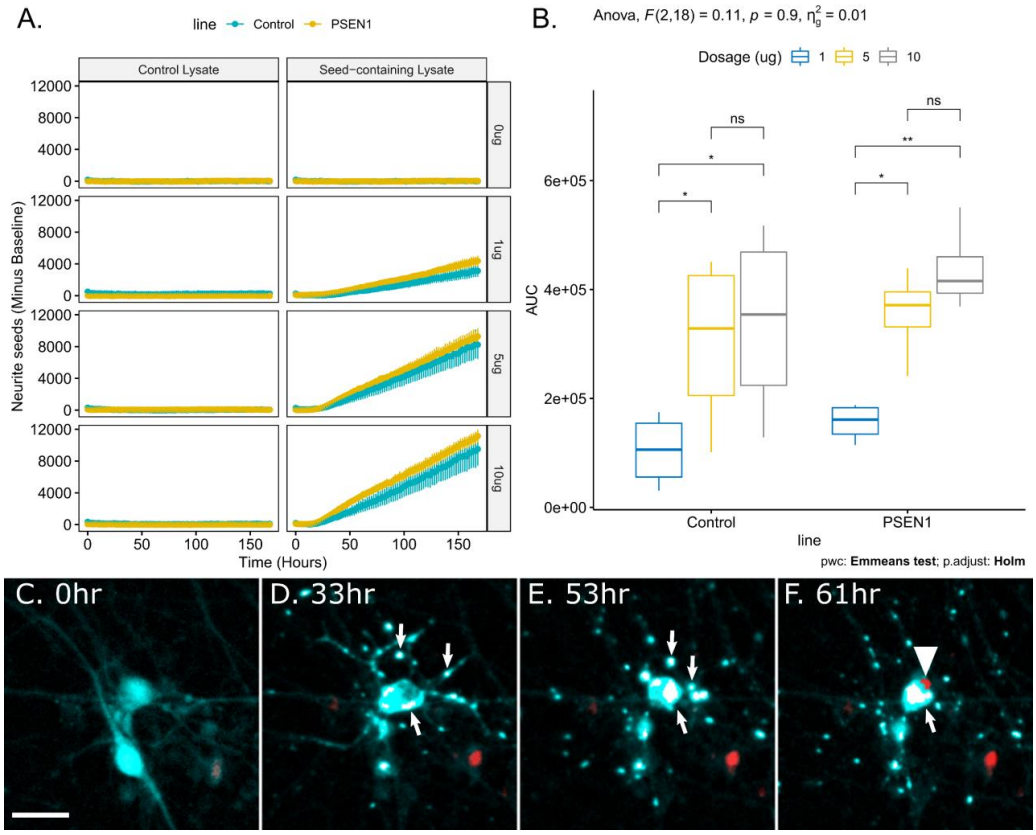

Fig 3. Live-imaging of neurite seeding and cell death in iPSC-neurons. (A-B) Graphs in A) depict the average number of TauRD-YFP reporter seeds within neurites per well for 7 days following addition of either seed-containing lysate (rTg4510) or control lysate, (+/- s.e.). n=3 independent neuronal differentiations for all experiments except control neurons paired with 1ug control lysate where n=2. Values represent the sum of two technical replicates per experiment. Subtracted baseline is the overall average number of events detected in the no-lysate condition for each line (quantification noise). B) Mean area under the curve for neurite seeding assay in (A) plotted for each dosage of seed-containing lysate, grouped by cell line. *p<=0.05, **p<=0.01. Two-way ANOVA results at top are for the interaction of cell line and dosage (n.s. p=0.9). (C-F) Following addition of tau seeds at 0hr (C), TauRD-YFP aggregation occurs beginning in neurites (D)(arrows), concentrating in cell body (E), and preceding neuronal death, highlighted by increased red signal from nuclear dye (arrowhead) (F). The cell body disappears following cell death. Cyan= TauRD-YFP, White = Tau-YFP aggregates (saturated, pseudocolored), Red=NucSpot 650 showing maximal signal at cell death. PSEN1 mutant iPSC-neurons used in this example. Scale bar = 25µM. See Extended Data Figures 3-1 & 3-2.

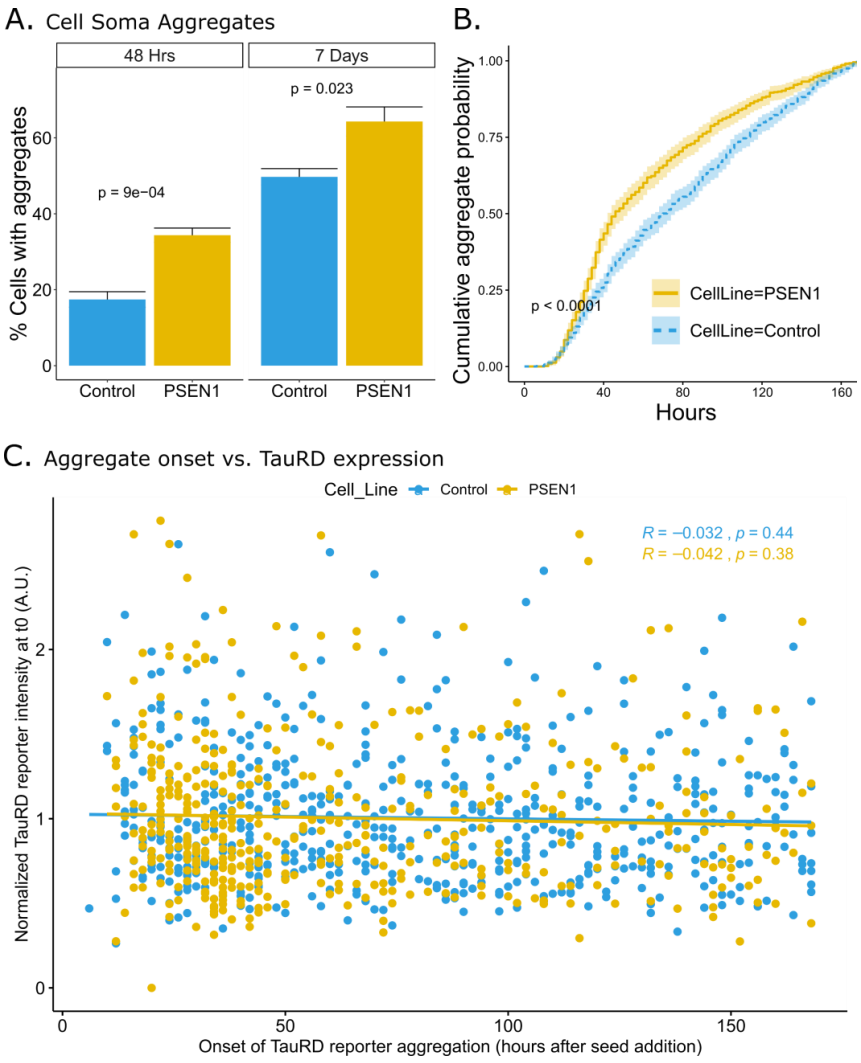

Fig 4. Accelerated aggregate formation in PSEN1 mutant iPSC-neurons. A) PSEN1 L435F mutant neurons show a higher percentage of TauRD-YFP cell soma aggregates compared to control at both 48 hours and 7 days after addition of 10µg seed material (p=0.0009 and p=0.0232 respectively, n=4 independent neuronal differentiations, +/- s.e.). B) Time course of soma aggregate formation in Control and PSEN1 L435F mutant iPSC-neurons. (p<0.0001, plots are +/- 95% confidence interval). C) Onset of TauRD reporter aggregation does not correlate with expression levels. The onset of TauRD reporter aggregation is plotted against normalized fluorescence intensity of the TauRD reporter per-cell at the first imaging timepoint (t0). Pearson correlation is plotted for each cell line. n=3 independent differentiations. In total, 591 Control neurons and 441 PSEN1 mutant neurons are depicted. Normalized t0 values correspond to the average TauRD fluorescence intensity in an ROI centered over the tracked neuron divided by the average fluorescence intensity of all tracked neurons in each replicate, per-cell-line. Neurons that do not develop TauRD aggregates are excluded from this analysis. See Extended Data Figure 4-1.

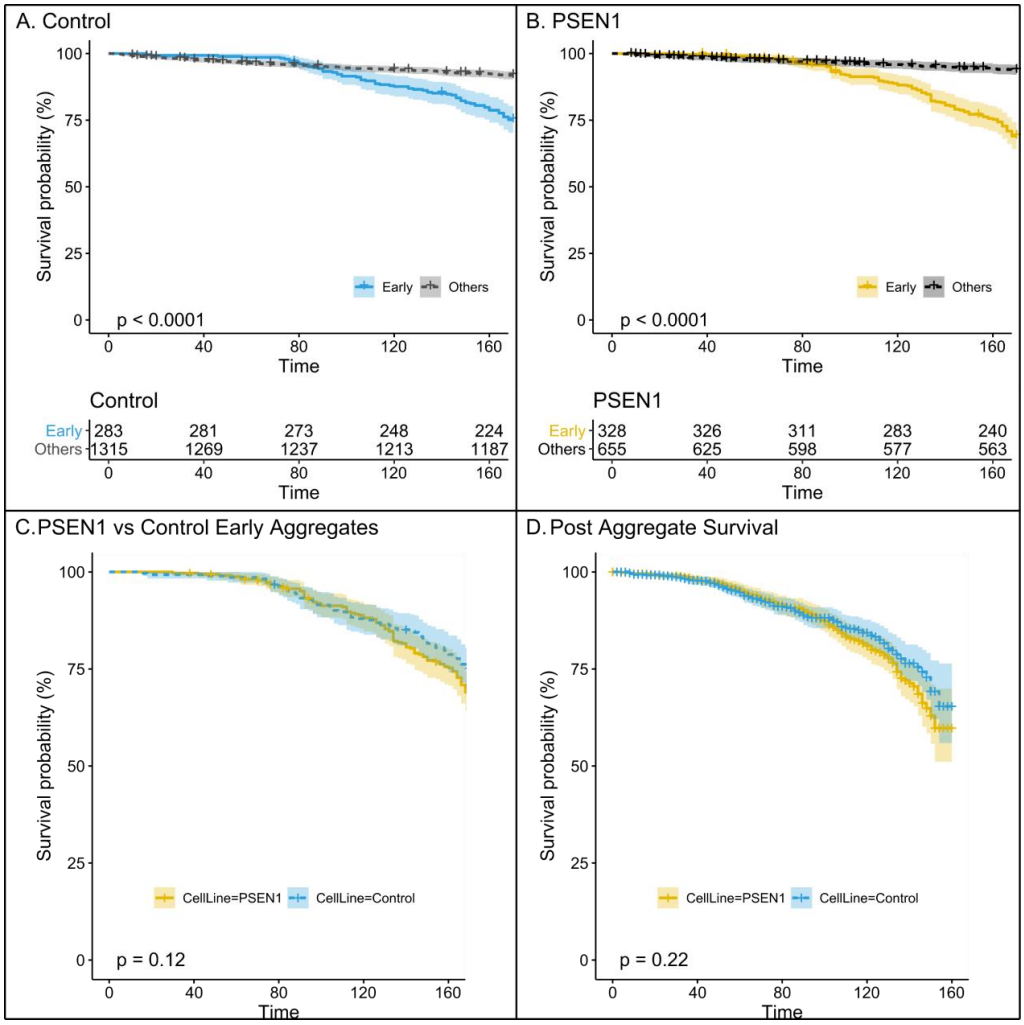

Fig 5. TauRD aggregate toxicity in Control and Familial AD iPSC-neurons A-B) Reduced survival in control (A) and PSEN1 L435F (B) neurons that form aggregates within 48 hours after addition of seeds (Early) compared to all other neurons in the same well (Others), including cells that develop aggregates at later timepoints ($p<0.0001$ for both (+) vs. (-) aggregate comparisons. n.s. for line comparison by log-rank test, n=4 independent neuronal differentiations, plots are +/- 95% confidence interval). Crosses indicate censored cells. Number at risk for each timepoint is presented below (A) and (B). Time is represented in hours after seed addition. C) Survival curves for early aggregate forming neuronal populations (less than 48 hours after seed material addition) from Control and PSEN1 mutant cells. D) Survival curves for all aggregate forming neurons from both cell lines beginning from the time of aggregate formation. Censor crosses are frequent in D due to censoring at the experimental endpoint, which occurs at a variable time with respect to aggregate formation in each cell. See Extended Data Figures 5-1, 5-2, & 5-3.

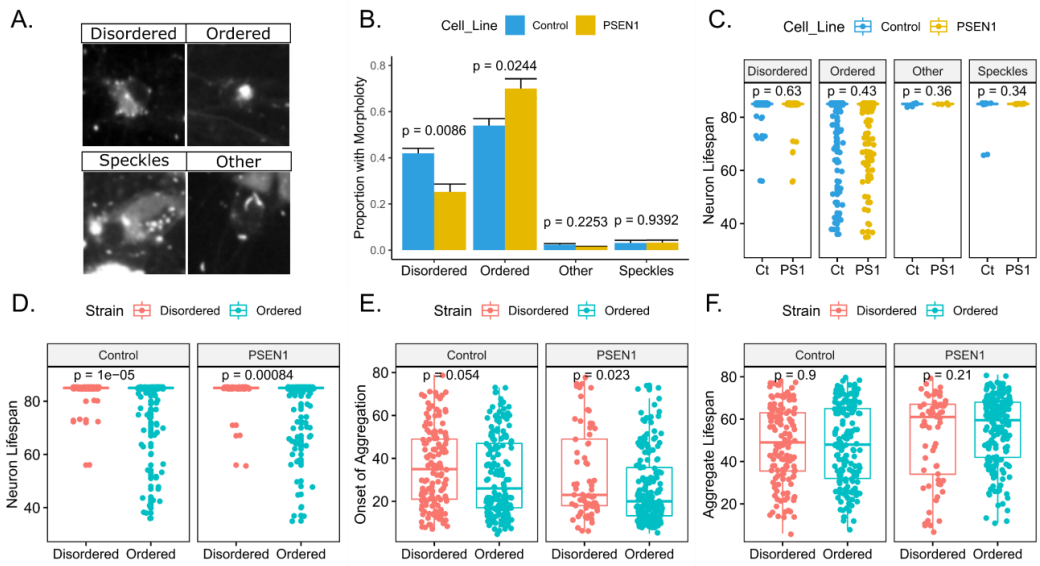

Fig 6. TauRD aggregate morphologies correlate with neurotoxicity. A) Example images of observed TauRD aggregate morphologies (n=322 control neurons and 267 PSEN1 L435F neurons). B) Relative proportions of each aggregate morphology for Control and PSEN1 cell lines +/- s.e. C-F Boxplots depicting: C) Neuronal lifespan in Control and PSEN1 iPSC-neurons with aggregates, grouped by aggregate morphology (Ct=Control, PS1=PSEN1). D-F) Comparison of neuronal lifespan (D), Onset of aggregation (E), and Aggregate lifespan (F) respectively for cells with disordered and ordered aggregates, grouped by cell line. In B-C, p values are for pairwise comparison between the two cell lines. In D-F, p values are for pairwise comparison between aggregate types.

805

Case	Age	Sex	Diagnosis	Mutation	Braak Stage	Thal Phase	CERAD Density	Diffuse Aβ	ApoE	Race
2012, C1	>90	F	Control	N/A	II	0	0	None	3/3	W
2048, fAD1	53	F	Familial AD	PSEN1 L435F (c.1303C>T)	VI	3	3	Frequent	3/3	W

806

807 **Table 1: Clinical characteristics of iPSC donors.** Braak, Thal, and CERAD staging as described(Hyman et
808 al., 2012), AopE=ApoE genotype.

809

810

Extended Data:

Fig 1-1: Karyotype and Flow Cytometry on iPSCs. Normal karyotype of Control (A) and PSEN1 L435F (B) iPSCs expressing the TauRD reporter. C) Flow Cytometry of Control (top) and PSEN1 (bottom) iPSCs demonstrating similar overall levels of TauRD-YFP expression and an absence of CFP-TauRD expression (attributed to recombination during reverse transcription and viral integration).

Fig 1-2: NGN2 directed differentiation produces high-purity layer II/III glutamatergic cortical neurons. (A) Neurons immunostained for the neuronal marker Tuj1 following live-imaging experiments (n=4 replicates matched to those used for live imaging experiments, without addition of brain lysate). Nuclear staining is Nucspot650 as used in live imaging. (B-C) Neurons immnostained at Day 14 of differentiation for (B) upper-layer cortical markers Cux1 and Brn2, Lower-layer cortical marker Ctip2 (C), and the glutamatergic neuron marker Tbr1 (C). Day 14 chosen to represent the population of neurons present at the start of live imaging experiments. Scale bar = 200µm (A) and 100 µm (B, C). (D) Quantification of TUJ1 positive cells as a percentage of all Nucspot650 stained nuclei at Day 21. p values are for Control vs. PSEN1 comparison (n=4 independent differentiations). (E) Quantification of neuronal fate markers in Day 14 TUJ1-positive neuronal nuclei shows a high percentage of BRN2, CUX1, and TBR1 positive neurons consistent with layer II/III glutamatergic cortical neurons. p values are for Control vs. PSEN1 comparison (n=2 independent differentiations). Error bars are +/- standard error.

Fig 2-1. Alexa-647-labeled rTg4510 brain lysate uptake and seeding at 5 days post seed addition in control iPSC-neurons. A.) TauRD aggregate formation (green) in response to labeled rTg4510 brain lysate addition into culture media (red). Nuclei are labeled with DAPI (Blue). B.) Labeled rTg4510 lysate only from panel (A). C.) Control condition identical to (A) except without addition of labeled rTg4510 seed material. D.) Red channel only from panel (C) (no rTg4510 lysate). E-G) 647-labeled rTg4510 lysate uptake measurement in TauRD reporter-expressing iPSC-neurons. Average 647-label intensity was calculated for the entire neuronal soma (E), the soma minus the nuclear compartment (F), and the nuclear compartment alone (G). Comparison of average intensity was then performed for TauRD aggregate-bearing neurons (n=26, Aggregate) vs non-aggregate-bearing neurons (n=65, NoAgg). No significant differences in 647 label uptake were identified between the two classes. Scale bar = 20µM.

Fig 3-1: Quantification of neurite aggregates: Example 10x fields of TauRD reporter-expressing iPSC-neurons immediately after (time 0) and 130 hours after (time 65) addition of rTg4510 lysate. Cyan ROIs indicate detected neurite aggregates. Objects at time 0 or without addition of lysate are false positives and subsequently subtracted from counts. Large objects (cell bodies, cell clusters, single large aggregates) are excluded from the analysis. Scale bar = 200µm.

Fig 3-2: Neurite density in Control and PSEN1 neurons. Top: original and WEKA segmented images as indicated. Grey values in the lower row represent the probability of segmentation into the background or neurite categories. Segmentation in the upper right image is created by thresholding the neurite probability without local background subtraction. Bottom: Quantification of average neurite area per image in neurite seeding assay +/- S.D. (n=3 independent neuronal differentiations, samples are matched to those in the neurite seeding assay and those with supernatant collected for Aβ species measurement).

Fig 4-1: Scored live imaging sample. Individual neuronal cells manually tracked using a custom ImageJ macro throughout the duration of a 7-day live imaging experiment and scored according to their ultimate phenotype. Image above is the first timepoint of live imaging. Cell class names in symbol key are composed of Initial_State+End_State+Survival_Status (i.e. O+A+D above) and colored yellow if censored during the live imaging experiment. For Initial_State and End_State A=TauRD reporter aggregate, O=no aggregate. For Survival_Status , A=Alive, D=Dead. “Trans” indicates transient aggregation. Cyan = YFP-TauRD reporter, Red = NucSpot 650 Nuclear dye.

Fig 5-1: TauRD reporter expression vs. lifespan. Intensity of TauRD reporter expression shows a weak positive correlation with lifespan in control neurons. The above analysis is restricted to cells that died during the experiments and includes cells both with and without TauRD aggregation. Neuronal lifespan is plotted against normalized fluorescence intensity of the TauRD reporter per-cell at the first imaging timepoint (t0). Pearson correlation is plotted for each cell line. n=3 independent differentiations. In total, 131 Control neurons and 135 PSEN1 mutant neurons are depicted. Normalized t0 values correspond to the average TauRD fluorescence intensity in an ROI centered over the tracked neuron divided by the average fluorescence intensity of all tracked neurons in each replicate, per-cell-line. Lifespan is represented in 2-hour increments after seed addition.

886

887

888 **Fig 5-2: TauRD aggregate toxicity in Control and Familial AD iPSC-neurons**. Survival curves for all
889 neurons forming aggregates from Control and PSEN1 mutant cell lines. Crosses indicate censored
890 cells. Number at risk for each timepoint is presented below. Time is represented in 2-hour increments
891 after seed addition.

892

Extended Data Figure 5-3: Cox proportional hazard model. Cox proportional hazard model comparing risk of cell death by cell line (PSEN1 mutant vs. Control) and time of cell soma aggregate formation (Early = prior to 48 hours after addition of seed material). Lower values indicate a reduced risk of cell death compared to the reference group.

Movie 1 (separate file): Video of aggregate formation and neuronal death in PSEN1 mutant neuron from figure 4. Imaging begins within one imaging interval (2hrs) following addition of 10ug rTG4510 brain lysate. Cyan = TauRD reporter, Red = NucSpot 650. Flash of increased NucSpot 650 brightness indicates membrane lysis and neuronal death.

Movie 2 (separate file): Video of the first 100 cell deaths in control iPSC neurons, with or without TauRD aggregation. Imaging begins within one imaging interval (2hrs) following addition of 10ug rTG4510 brain lysate. Cyan = TauRD reporter, Red = NucSpot 650. Flash of increased NucSpot 650 brightness indicates membrane lysis and neuronal death. Data is combined from 4 independent neuronal differentiations.

Movie 3 (separate file): Video of the first 100 cell deaths in PSEN1 L435F iPSC neurons, or and without TauRD aggregation. Imaging begins within one imaging interval (2hrs) following addition of 10ug rTG4510 brain lysate. Cyan = TauRD reporter, Red = NucSpot 650. Flash of increased NucSpot 650 brightness indicates membrane lysis and neuronal death. Data is combined from 4 independent neuronal differentiations.